Bioinspired Interlocked and Hierarchical Design of ZnO Nanowire Arrays for Static and Dynamic Pressure-Sensitive Electronic Skins

*Minjeong Ha, Seongdong Lim, Jonghwa Park, Doo-Seung Um, Youngoh Lee, and Hyunhyub Ko**

The development of electronic skin (e-skin) is of great importance in human-like robotics, healthcare, wearable electronics, and medical applications. In this paper, a bioinspired e-skin design of hierarchical micro- and nano-structured ZnO nanowire (NW) arrays in an interlocked geometry is suggested for the sensitive detection of both static and dynamic tactile stimuli through piezoresistive and piezoelectric transduction modes, respectively. The interlocked hierarchical structures enable a stress-sensitive variation in the contact area between the interlocked ZnO NWs and also the efficient bending of ZnO NWs, which allow the sensitive detection of both static and dynamic tactile stimuli. The flexible e-skin in a piezoresistive mode shows a high pressure sensitivity (–6.8 kPa^{-1}) and an ultrafast response time (<5 ms), which enables the detection of minute static pressure (0.6 Pa), vibration level (0.1 m s^{-2}), and sound pressure (≈57 dB). The flexible e-skin in a piezoelectric mode is also demonstrated to be able to detect fast dynamic stimuli such as high frequency vibrations (≈250 Hz). The flexible e-skins with both piezoresistive and piezoelectric sensing capabilities may find applications requiring both static and dynamic tactile perceptions such as robotic hands for dexterous manipulations and various healthcare monitoring devices.

1. Introduction

The development of electronic skin (e-skin) has received much attention owing to its potential use in various applications including robotics, prosthetic limbs, healthcare monitoring, wearable electronics, and medical diagnosis.[1–15] However, e-skins developed thus far are not as flexible, sensitive, and responsive as the human skin. The large sensory organ of the human body, the skin, enables the sensation of physical touch, vibration, textures, and hardness through various types of tactile receptors. In particular, the human skin can discriminate between static and dynamic mechanical stimuli owing to the different types of embedded mechanoreceptors such as Ruffini organs and Pacinian corpuscles. While the slowly adaptive Ruffini organs are suitable for static perception, involved in processes such as grasping objects with constant pressure, the rapidly adaptive Pacinian corpuscles usually perceive dynamic stimuli, such as those associated with high-frequency vibrations.[16–18] To mimic the sensing capabilities of the human skin, several types of highly sensitive e-skins have been developed.[19–22] Capacitive or resistive e-skins have been introduced for the perception of static mechanical stimuli through continuous electrical response of active sensing elements,[2,20,21,23] whereas the relatively fast response of piezoelectric and triboelectric e-skins have been shown to respond to dynamic stimuli via instantaneous charge generation.[11,16,24]

Typical sensing materials used in e-skins include dielectric elastomers, such as high-*k* polymers,[25,26] conductive polymers (poly(3-hexylthiophene), polypyrrole, polyaniline),[12] or semiconducting (Si, ZnO, and CdSe) and metallic (carbon nanotube (CNT), graphene, Au, and Ag) nanomaterials embedded in elastomers.[3,6,19,27] However, elastomers with viscoelastic behavior result in a delayed response time (≈10 s) and a large hysteresis.[28–30] In addition, the large thermal expansion of polymers causes temperature-dependent changes in the intrinsic electrical properties.[31,32] To overcome these fundamental limitations of traditional e-skins with monofunctional and planar structures, novel geometrical designs of e-skin structures should be introduced for the effective transduction of external stress into electrical signals.

Biological systems in nature have efficiently evolved their micro- and nano-structures to maximize their unique structural functions in response to environmental changes. Examples of sophisticated hierarchical morphologies in organisms include the strong adhesion of gecko's foot,[33] tight connection of the head arrester in dragonflies,[34] locomotion with high frictional force of a lizard's tail,[35] and remarkable absorptivity of the human intestinal villi,[36] where the hierarchical structures increase the surface area and enable conformal contacts. While nature provides many structural functions, which can be employed in the design of e-skins, there have been only a few attempts to mimic these biological morphologies in the development of high-performance e-skins. Pang et al. reported on highly sensitive, multiplex strain sensors based on interlocked nanofiber arrays that mimic the wing-to-body locking microstructures in

M. Ha, S. Lim, J. Park, D.-S. Um, Y. Lee, Prof. H. Ko
School of Energy and Chemical Engineering
Ulsan National Institute of Science and Technology (UNIST)
Ulsan Metropolitan City 689-798, Republic of Korea
E-mail: hyunhko@unist.ac.kr

DOI: 10.1002/adfm.201500453

beetles.[4] Maschmann et al. developed omnidirectional air-flow sensors using artificial CNT-hair arrays,[37] which resemble the sensory hairs of crickets,[38] locusts,[39] and bats,[40] in the natural world. We recently showed multidirectional-force-sensitive e-skins mimicking the interlocked microstructures between the epidermal–dermal layers of human skin.[41]

Inspired by both the hierarchical and interlocked structures of biological systems, here we develop highly-sensitive and rapidly-responsive e-skins based on the interlocked geometry of hierarchical micro- and nano-structures of polydimethylsiloxane (PDMS) micropillars decorated with ZnO nanowire (NW) arrays. In particular, we demonstrate that our e-skins can be utilized in the detection of both static and dynamic tactile signals due to the piezoresistive and piezoelectric properties, respectively, of ZnO NWs. Through the geometrical design of the interlocking system[3,4] between the hierarchical ZnO NW arrays, the effective contact area between NWs can be significantly varied in response to the external stimuli, which results in the highly sensitive piezoresistive static sensors. In addition, the hierarchical NW arrays on the micropillars exhibit extremely sensitive bending of ZnO NWs, enabling the piezoelectric perception of instantaneous dynamic tactile stimuli. The hierarchical assembly of rigid crystalline ZnO NWs provides an ultrafast response with minimal hysteresis, which cannot be achieved with conventional pressure sensors that use viscoelastic polymers.[28–30] Moreover, the relatively low thermal expansion of ZnO NWs[42] and the hierarchical structure of e-skin enables a thermally stable and reproducible pressure sensing capability. Finally, we also demonstrate that our hierarchical design can be applied to perceive dynamic stimuli associated with high frequency vibration.

2. Results and Discussion

2.1. Fabrication of Hierarchical ZnO NW Arrays

To design the interlocked geometry of hierarchical micro- and nano-structures for flexible e-skins, we fabricated hierarchical ZnO NWs on PDMS micropillar arrays (**Figure 1**a). This simple solution-based hydrothermal method enables a low-cost,

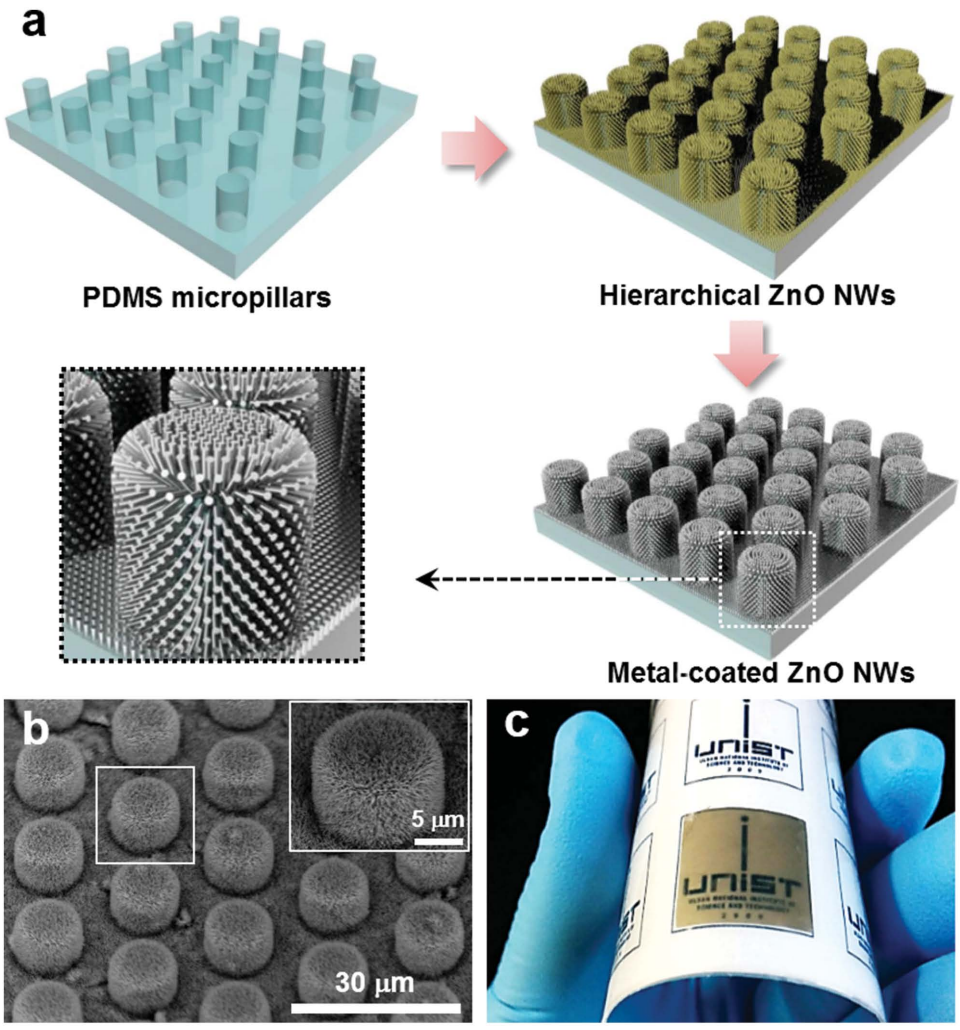

Figure 1. Bioinspired hierarchical ZnO NW arrays. a) Schematic illustration of the fabrication of metal-coated ZnO NWs on PDMS micropillars. b) A tilted SEM image of ZnO NWs (diameter: ≈50 nm and aspect ratio (AR): 20) on the PDMS micropillars (diameter: ≈10; height: ≈10; and pitch: ≈20 μm). c) A photograph showing the highly flexible and optically transparent properties of metal-coated hierarchical ZnO NW arrays.

large-area, and low-temperature fabrication of ZnO NW arrays with high aspect ratio (AR) and precisely controlled dimensions on flexible polymer substrates with arbitrary surface morphologies. In this fabrication process, first, PDMS micropillar arrays were molded from microhole-patterned silicon (Si) micromolds. Then, ZnO NWs were grown on top of the PDMS micropillar arrays by using a hydrothermal method. Finally, the hierarchical structures were coated with thin metal films to increase the electrical conductivity, thus increasing the piezoresistivity. A scanning electron microscopy (SEM) image in Figure 1b shows that ZnO NW arrays were uniformly grown on top of the PDMS micropillar arrays by using a hydrothermal method. For the solution-based hydrothermal growth of ZnO NWs (Figure S1a, Supporting Information), ZnO nanocrystal nucleation sites were uniformly coated on the PDMS micropillar arrays by using a dip-coating method. Then, the PDMS substrates were floated onto the surface of the growing solution with the micropillar side facing downward in the solution for the uniform growth of ZnO NWs without the formation of any ZnO precipitates. During the growth of ZnO NWs, zinc cations (Zn^{2+}) from zinc nitrate hydrate ($Zn(NO_3)_2 \cdot xH_2O$) and oxygen anions (O^{2-}) from distilled (DI) water were alternatively stacked along the *c*-axis of ZnO NWs.[43] The X-ray diffraction (XRD) analysis indicates that the grown ZnO NWs exhibited hexagonal wurtzite structures with the highest (002) plane peak for *c*-axis crystal growth direction and minor peaks for the (100), (101), and (102) planes for hexagonal symmetry (Figure S1b, Supporting Information). Because the semiconducting ZnO NWs with a large direct band-gap (≈3.3 eV) show a high electrical resistance (≈10^9 Ω),[42,44,45] thin metal (Pt, Ni) film coatings on top of ZnO NW arrays can reduce the electrical resistance from that of the pure sample by a factor of at least ≈10^{-3}, thus facilitating the current flow between ZnO NWs. Figure 1c shows that metal-coated hierarchical ZnO NW arrays are flexible and optically transparent. In our design of e-skins based on interlocked and hierarchical micro- and nano-structures, contrary to conventional conductive composite films,[19,3] the piezoresistivity is mainly affected by the stress-induced change in contact area between the interlocked hierarchical structures. Therefore, the dimensions of the ZnO NWs and PDMS micropillar arrays significantly affect the deformation-induced change in contact area and thus affect the overall performance of the e-skin. In this study, we systematically vary the AR of ZnO NWs (Figure S1c,d, Supporting Information) and the pitch size (20, 30, and 40 μm) of the PDMS micropillar arrays (Figure S2, Supporting Information), to investigate their effect on the sensing performance of our e-skins (Figure S3, Supporting Information).

2.2. Piezoresistive E-Skins with Static Pressure-Sensing Capabilities

Figure 2a illustrates the device configuration, wherein we can see the interlocked geometry of hierarchical micro- and nanostructures for highly sensitive piezoresistive e-skins. The SEM image in Figure 2b clearly shows that the top and bottom ZnO NWs on the PDMS micropillar arrays are interlocked with each other. In this interlocked geometry, an applied pressure induces a change in the contact area between the interlocked NWs, thus changing the contact resistance (Figure S4, Supporting Information). In particular, the large surface area provided by the hierarchical structures of ZnO NWs on the PDMS micropillar arrays can induce a great change in contact resistance. Further, the hierarchical geometry enables minimal contact between NWs without any application of pressure and a continuous increase in contact area with the application of pressure, thus leading to highly sensitive piezoresistivity in e-skins.

To verify the relationship between the structural geometry and pressure sensitivity of these hierarchical NW arrays, we compared the piezoresistivity of hierarchical NW arrays coated on micropillar arrays with varying pitch sizes and that of planar NW arrays without hierarchical structures. Figure 2c shows that the relative resistance of e-skins decreases rapidly with the increase in normal pressure at low-pressure regimes (below 2 kPa), then decreases slowly at a high-pressure regime (over 2 kPa). For different pitch sizes of micropillar arrays, the largest decrease in resistance is observed in the sensor with the smallest pitch size (20 μm), which is 3.7 times more pressure-sensitive (–6.8 kPa^{-1}) than planar NW arrays (–1.8 kPa^{-1}) at pressures below 0.3 kPa (Table S1, Supporting Information).

The change in resistance with the pitch size of the micropillar arrays shows a nonlinear dependence on pressure, which can be attributed to the nonlinear relationship between the applied pressure and the inter-NW contact area.[3,46] The gradual decrease in sensitivity, corresponding to a nonlinear power law, is advantageous in increasing the dynamic range of the pressure sensor for the detection of high-pressure stimuli.[3,47] The nonlinear dependence of resistance on pressure can be fit using a power-law function $y = ax^{-b}$ (Figure 2c). As can be seen in Figure 2d, exponent b (= 0.64 for a 20 μm pitch sensor) decreases with increasing micropillar pitch, finally reaching a value of 0.17 for planar ZnO NWs with an infinite pitch size. For elastic deformation of typical contacting surfaces, exponent b is known to be proportional to the surface roughness and thus the surface area.[46,48,49] In our study, exponent b is proportional to the density of the hierarchical structures, which is also shown to be proportional to the sensitivity of piezoresistive e-skins. Exponent b decreases further with a decrease in the AR of ZnO NWs, reaching a value of 0.02 for ZnO NWs with an AR of 5 (Figure 2d). Therefore, exponent b in our study indicates the sensitivity of piezoresistive e-skins, which is directly related to the surface area of the structured surfaces. For practical sensor applications, the nonlinear dependence of resistance on pressure can be linearized by using a log–log scale plot (Figure S5, Supporting Information). The hierarchical ZnO NW arrays with an optimized micropillar pitch (20 μm) and a NW AR (20) are capable of detecting a small water droplet (Figure 2e). The detection limit is below 0.6 Pa, which is lower than that of recently reported nanofiber-interlocked sensors (≈3 Pa).[4]

Mechanical durability and thermal stability are important issues in the development of reliable and robust e-skins. The hierarchical design of e-skins provides enhanced mechanical durability compared with e-skins based on planar design. As can be seen in **Figure 3**a, with repeated pressure loadings (13 kPa), the hierarchical NW structures show a consistent change in relative resistance from 1 at 0 kPa to 0.045 at 13 kPa. On the contrary, the planar NW structures exhibit unstable variation of relative resistance, where the relative resistance decreases to 0.25 at

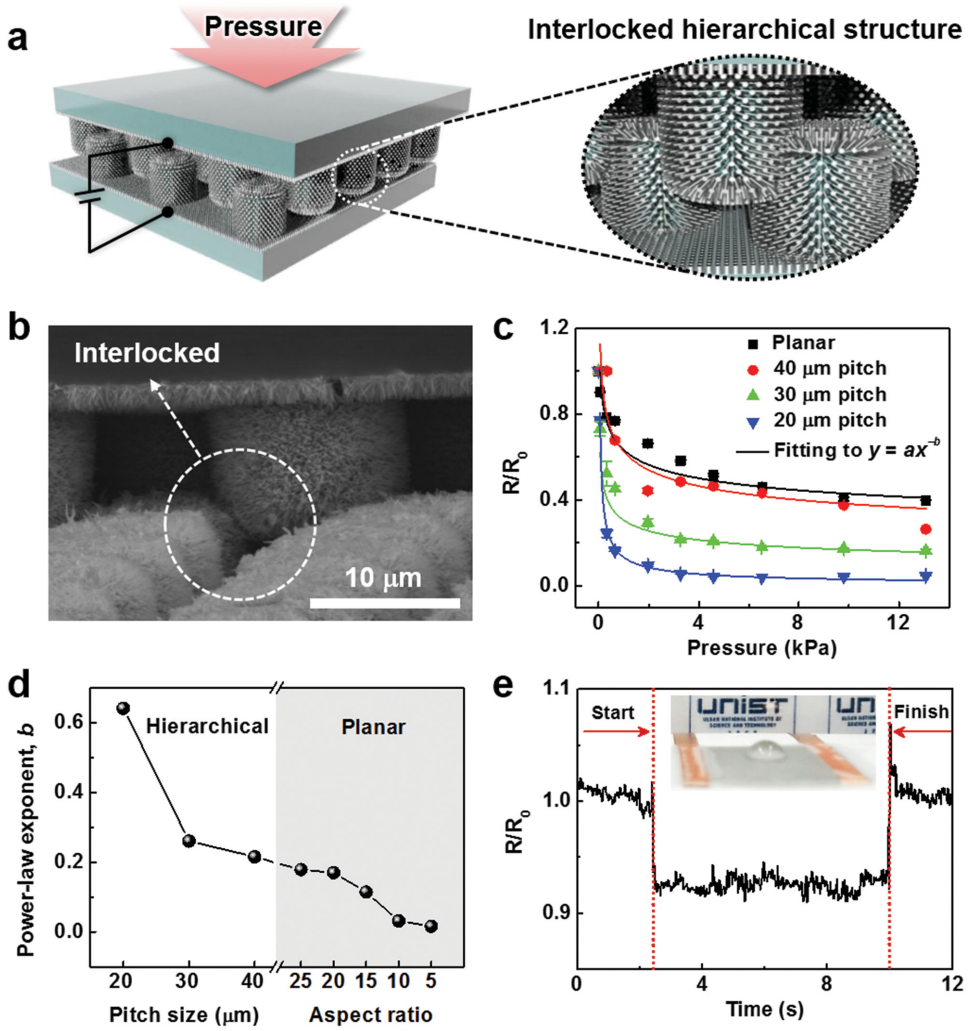

Figure 2. Static-pressure-sensing capability of e-skins based on the interlocking geometry of hierarchical ZnO NW arrays. a) Schematic illustration of the piezoresistive e-skin device based on the interlocking geometry of hierarchical ZnO NW arrays. b) A cross-section SEM image of interlocked NWs on the PDMS micropillar arrays. c) Change in relative resistance as a function of normal pressure for different pitch sizes of e-skins. The solid lines are the power-law fittings to $y = ax^{-b}$. d) Variation in exponent b in the power-law fitting as a function of micropillar pitch size and AR of ZnO NWs. e) Minimum detection capability of e-skins showing the detection of a small water droplet (0.58 Pa) on the e-skin.

13 kPa, but it does not come back to the original value ($R/R_0 = 1$) when the applied pressure is released. The increased mechanical durability of hierarchical structures compared with planar structures can be attributed to the reduced crack formation in the conductive Pt films. As can be seen in Figure S6 (Supporting Information), for planar NW structures, the repeated pressure loadings induce the formation and propagation of surface cracks arising from the difference in moduli between the Pt-coated ZnO NW arrays and the PDMS surface. On the contrary, the micropillar arrays employed in hierarchical NW structures can efficiently prevent crack formation and propagation. We also observed no delamination between the ZnO NWs and micropillar-patterned PDMS substrates. It has been reported that the propagation of the surface crack can be prevented by the protruding microstructures.[50,51] The low mechanical durability of planar structures also affects the pressure sensitivity. As can be seen in Figure S7 (Supporting Information), the pressure sensitivity of planar structures continuously decreases with the repeated pressure loadings (1000 cycles). However, the hierarchical structures exhibit a minimal change in pressure sensitivity with the repeated pressure loadings. It is also worth to note that the high mechanical flexibility of ZnO NW[52] permits the repeated bending of interlocked ZnO NWs, resulting in high mechanical durability of surface nanostructures.

The decreased formation of surface cracks in hierarchical structures is also advantageous in the thermal stability of e-skins. For planar structures, the thermal expansion of PDMS with temperature variation, in the range of 30–90 °C, results in crack formation and the subsequent fluctuation in pressure sensitivity, which depends on the temperature. However, for the same temperature range, the increased thermal stability of hierarchical ZnO NW arrays with minimal crack formations results in a stable pressure sensitivity (error rate <0.05%) compared with the planar one (error rate <8.5%) (Figure 3b). The higher

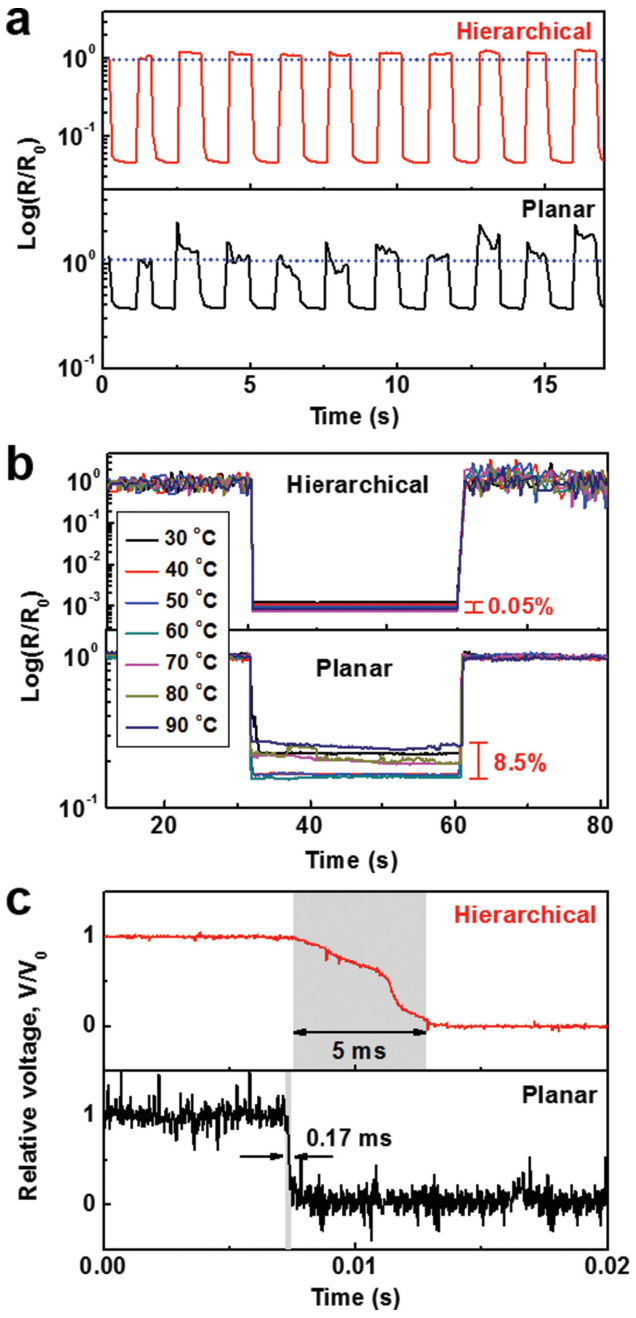

Figure 3. Mechanical durability, thermal stability, and response time of hierarchical and planar ZnO NW arrays. a) Mechanical durability of hierarchical and planar ZnO NWs with repeated pressure loadings (13 kPa). b) Temperature stability of hierarchical and planar structured ZnO NWs for a temperature range of 30–90 °C. c) Response time of hierarchical and planar ZnO NW arrays.

temperature stability of hierarchical e-skins compared with that of planar ones can be also verified by the minimal change in current–voltage (I–V) curves for different temperatures (Figure S8, Supporting Information). The temperature-stable performance of our e-skins is in clear contrast to previously reported resistive-type sensors based on bulk composite films mixed with conductive materials such as metal particles, graphene, CNT, conductive polymers, where the pressure sensitivity is thermally unstable, mainly due to the thermal expansion of the polymer matrix.[31,32]

Our resistive-type sensor using an interlocking system shows a fast response time owing to the immediate change in contact area between the rigid crystalline ZnO NWs without viscoelastic deformation behavior. For most e-skins based on polymeric materials or their hybrid structures with inorganic materials, the response time is limited by the viscoelasticity of polymers.[28,29] However, in our e-skins based on the change in contact area between ZnO NWs, the recorded response time was ≈5 ms for hierarchical structures and 0.2 ms for planar ones (Figure 3c). This response time is much faster than those stated in recent reports with the fastest response time of ≈10 ms.[5,10] The faster response time of planar e-skins compared with hierarchical ones is attributed to the nonexistent viscoelastic behavior of PDMS micropillar arrays underneath the ZnO NWs.

Our interlocked films using hierarchical ZnO NWs are suitable for the detection of vibration stimuli. In **Figure 4**a, we illustrate the experimental setup of the vibration-motion sensing test. The small coin-like vibration motor is attached to the upper part of the interlocked films. Once the motor is vibrated from the external power, the vibrometer, which is directly connected to the vibration table, reads the exact intensity of the given vibration to the interlocked films. The results of electrical resistance variation demonstrate the exact responses of interlocked NW arrays depending on the vibration intensity (Figure 4b). For different levels of vibration intensity, the vibrational sensitivity in hierarchical structures (≈0.79/(m s^{-2})) was about 1.7 times higher than that of planar-type (≈0.47/(m s^{-2})) e-skins. The higher vibration sensitivity of hierarchical structures can be attributed to the larger surface area, and thus the contact area, between the interlocked structures. Our e-skins can also detect sound waves, i.e., acoustic vibration, encountered in daily life. The sound detection capability of e-skins is advantageous in various applications, including devices for hearing-impaired persons. Figure 4c represents the real-time monitoring of sound variations for different sound pressure levels (SPLs). With a gradual increase in SPL (57–90 dB), the interlocked hierarchical structures show a gradual increase in the fluctuation of relative resistance, indicating the capability of dynamic sound detection. The relative resistance change clearly represents a linear increase with respect to the increase of SPL (Figure 4d). The linear fitting to these data results in the sound pressure sensitivity ($(-\Delta R/R_0)/\Delta P_S$) of 0.02 dB^{-1} and a minimum SPL detection of ≈57 dB, which is comparable with the SPL of normal conversation (≈60 dB).[53] The linear relationship between the e-skin resistance and the SPL indicates that our e-skins can provide the exact information of sound intensity regardless of the frequency of sound, which is not the case for previous acoustic sensors based on piezoelectric and triboelectric transduction modes, where the sound intensity and frequency simultaneously affect to the signal amplitude.[54,55]

2.3. Piezoelectric E-Skins for Fast Dynamic Pressure-Sensing Capabilities

We further explored our hierarchical ZnO NW arrays for piezoelectric detection of high-frequency pressure variations. The

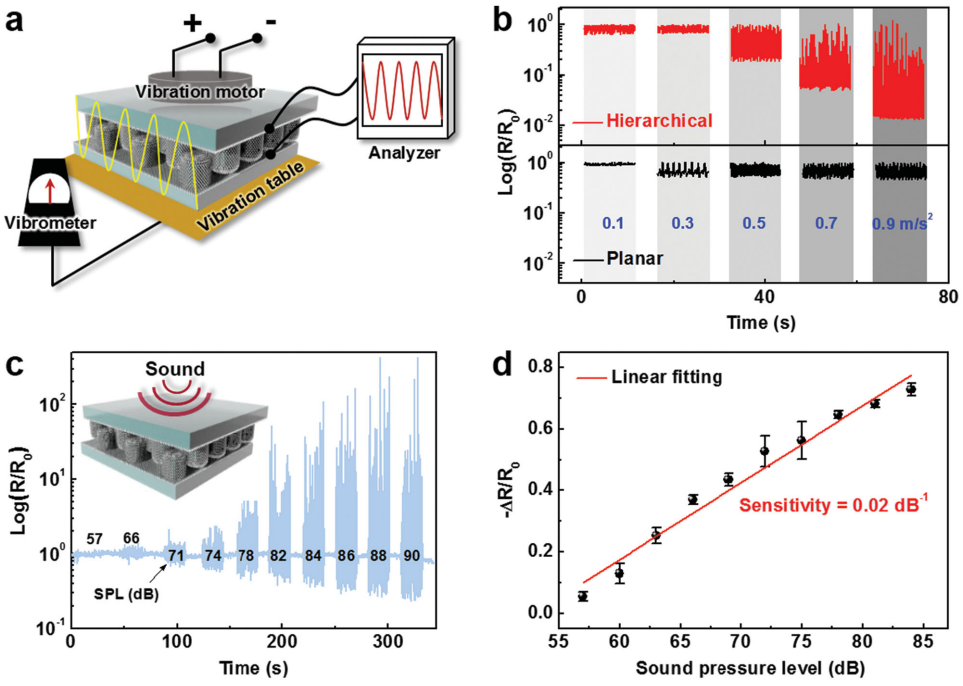

Figure 4. Vibration and sound sensing capabilities of e-skins. a) Schematic illustration of vibration measurements based on hierarchical ZnO NWs. A vibration motor provides input oscillations, the vibrometer measures the intensity of vibration, and the analyzer shows the output resistance change. b) Change in relative resistance of e-skins in response to various vibration intensities. c) Real-time monitoring of the sound-sensing capability of hierarchical NW arrays for different SPLs. d) The sound pressure sensitivity of hierarchical e-skins depending on the SPL values.

generation of piezoelectricity is a useful transduction method that converts external stimuli into electrical potential differences.[56,57] Especially, hexagonal ZnO is a representative piezoelectric material that shows a spontaneous polarization along the *c*-axis crystal direction.[45,58] **Figure 5**a illustrates the operating principle of our piezoelectric e-skins, in which the upper layer of hierarchical ZnO NW arrays in interlocked films was coated with Ni films (≈300 nm), and the bottom layer was comprised of bare hierarchical ZnO NW arrays. The Ni coating on one side of the interlocked films enables the formation of a Schottky barrier between the metal-coated NWs and the bare semiconducting NWs due to the difference between the Ni work function (5.5 eV) and the ZnO electron affinity (4.5 eV).[44,59] When a pressure is applied on top of the interlocked and hierarchical ZnO NW arrays, the unique geometry of interlocked and hierarchical ZnO NW arrays enables the efficient bending of large amount of ZnO NWs, where the relatively rigid, metal-coated NWs can press and bend the less rigid, bare NWs. The bending of bare NWs spontaneously induces a positive piezoelectric potential (V^+) on the stretched side of the ZnO NWs and a negative piezoelectric potential (V^-) on the compressed side of the NWs (inset (ii) in Figure 5a). Then, the spontaneously generated electron flows from the bare NWs to the metal-coated NWs owing to the forward-biased Schottky contact between the metal-coated NWs and the compressed side of the ZnO NWs with a negative piezoelectric potential.[59,60]

Figure 5b,c shows the output current density and voltage in response to the gradual increase in normal pressure applied on the interlocked films, which demonstrate the generation of electrical charge in the compressed state and the compensation of built-up charges in the released state. The output performance of current density and voltage is significantly increased with the increase in pressure, which is attributed to the compression of a larger number of NWs to a higher bending degree and the subsequent generation of a higher spontaneous electrical potential. In comparison with planar-type e-skins that exhibit a minor piezoelectric effect due to the inefficient bending of NWs,[61] the hierarchical NWs enable the efficient bending of NWs in response to normal pressure, and thus, result in the enhanced power output (≈5.9 mW m^{-2}, 11 times higher than that of the planar type (≈0.5 mW m^{-2})) and excellent pressure-sensing performance. In particular, we observe that both planar and hierarchical NWs in piezoelectric modes show a great mechanical durability for the repeated compression cycles (>1000 times) (Figure S9, Supporting Information). The efficient power generation observed in hierarchical structures can be potentially beneficial in the development of self-powered e-skin sensors.[62] Our hierarchical ZnO NW arrays present an output power comparable with that of other reported power generating devices that use native ZnO NWs. For example, our hierarchical NW arrays have an output power 2.5 times higher than that obtained for the hybrid structure of ZnO NWs on microfibers by Qin et al. (2.4 mW m^{-2}).[60]

Piezoelectric tactile sensors quickly respond to the external dynamic pressure owing to the instantaneous generation of piezoelectric signals via the separation of dipoles.[45] On the contrary, piezoresistive tactile sensors cannot detect high-frequency pressure variations owing to the time delay and differences in magnitude between the input and output responses with increasing frequency.[63] In Figure 5d, a pushing tester was utilized to provide

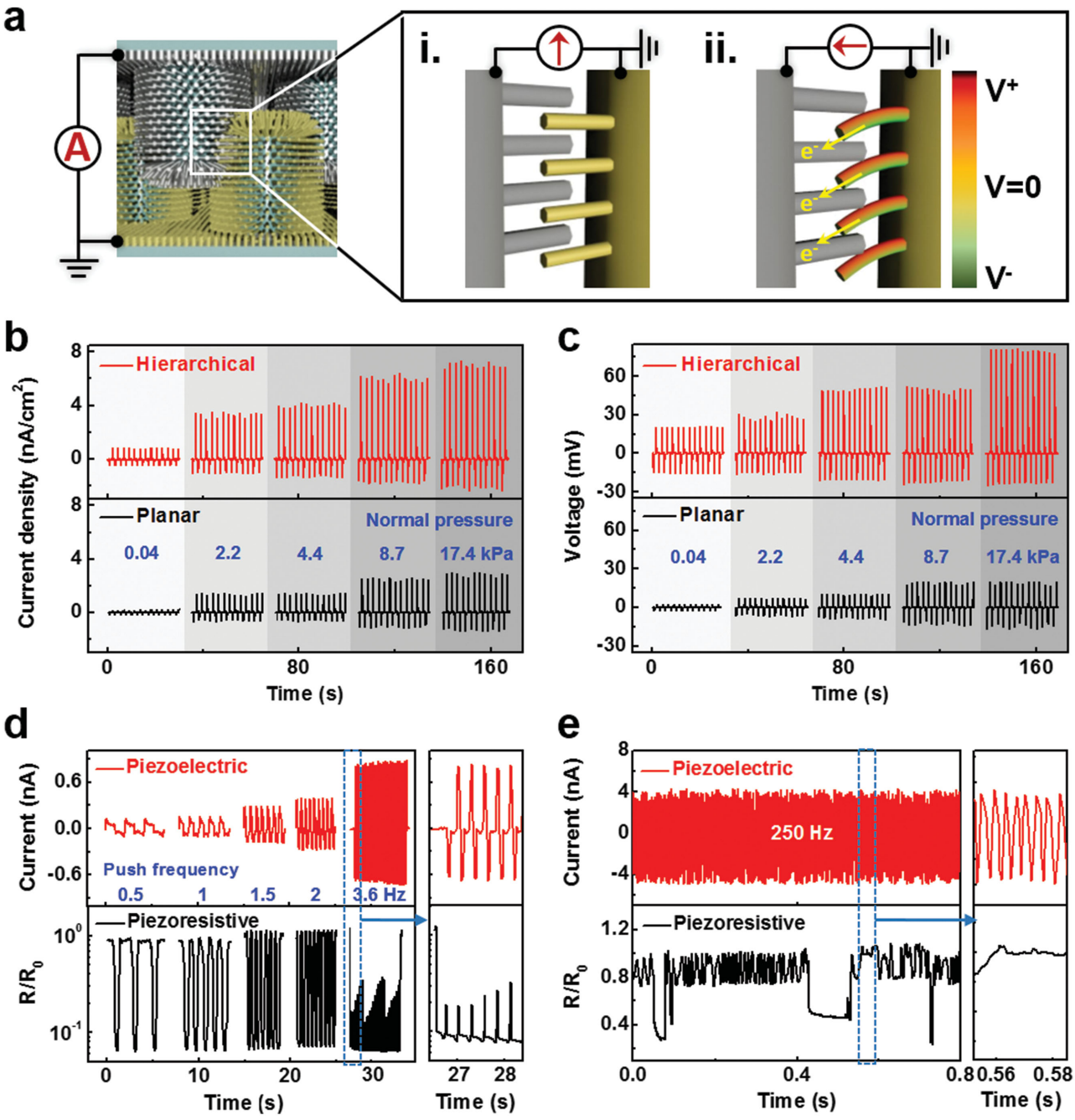

Figure 5. Piezoelectric performance of planar and hierarchical ZnO NW arrays. a) Schematic illustration of piezoelectric potential generation between the interlocked ZnO NWs (magnified in state i). The applied pressure bends the bare ZnO NWs and creates a piezoelectric potential (state ii). b) Output current density. c) Voltage of e-skins based on hierarchical and planar ZnO NWs depending on the applied pressure. d) Dynamic sensing performance of piezoelectric and piezoresistive e-skins depending on the vibration frequency. e) The high-frequency vibration sensing capability of piezoelectric e-skins.

a mechanical vibration with variable frequency on e-skins. While the piezoresistive e-skins cannot differentiate the vibration frequency at 3.6 Hz, the output current signals of piezoelectric e-skins increase with the increase in frequency from 0.5 to 3.6 Hz and clearly detect the frequency at 3.6 Hz. The generated current in piezoelectric e-skins can be represented as $I = d_{33}EA\dot{S}$, where d_{33} is the piezoelectric charge constant of ZnO NWs by the strain in the 3-direction (z-axis), E is the Young's modulus, A is the surface area of the NWs, and $\dot{S}$ is equal to the strain rate $S/\Delta t$.[13,64,65] From this equation, we anticipate that the strain rate of NWs is closely related to the piezoelectric output performance regardless of other fixed variations. When we applied high-frequency pressure variations, which reduced the time interval (Δt), the generation of output current was improved

by increasing strain rate ($\dot{S}$). In Figure S10 (Supporting Information), we calculated the theoretical current values using the known ZnO piezoelectric charge constants (d_{33}: 9.93 pm/V,[66] 12 pC/N[67]), which closely match with the experimental results with a linear dependence of current on the frequency. To further evaluate the high frequency vibration detection capability of flexible piezoelectric e-skins, a vibration motor was attached on the e-skins. Figure 5e shows that the piezoelectric e-skins can detect high-frequency vibration stimuli up to 250 Hz, which is well above the frequencies achieved with the previous flexible sensors such as piezoelectric sensor (≈60 Hz),[68] triboelectric sensor (≈10 Hz),[69] resistive pressure sensor (≈5.5 Hz),[8] and optical tactile sensor (≈16 Hz).[70]

3. Conclusion

In summary, we developed highly sensitive and ultrafast e-skins using bioinspired hierarchical ZnO NW arrays with interlocked geometry. We demonstrated that our interlocked and hierarchically structured e-skins enabled the sensitive detection of both static and dynamic stimuli through piezoresistive and piezoelectric transductions, respectively. We showed that the interlocked and hierarchical ZnO NW arrays could detect the extremely small stimulus of static perception as well as the dynamic stimuli such as minute vibration and sound stimuli. As contrary to the previous flexible sensors based on piezoelectric or triboelectric transduction modes, the dual mode e-skins based on piezoresistive and piezoelectric transductions enabled the detection of both intensity and frequency of sound stimuli. Furthermore, our flexible e-skins in a piezoelectric mode can detect high-frequency vibration (250 Hz), which is not achievable with previous flexible sensors. We anticipate that our flexible e-skins with both piezoresistive and piezoelectric sensing capabilities can find applications requiring static and dynamic tactile perceptions such as robotic skins, prosthetic limbs, and rehabilitation programs to monitor static and dynamic tactile and strain information.

4. Experimental Section

Fabrication of PDMS Micropillar Arrays: PDMS micropillar arrays were fabricated by mixing a PDMS base (Sylgard 184, Dow Corning) and a curing agent (Sylgard 184, Dow Corning) in a 10:1 ratio, and pouring the mixture into the micro-hole-patterned Si molds. Micro-hole arrays of different pitch sizes were fabricated by a conventional photolithographic technique with a dry etching process. In addition, the micro-hole-patterned Si molds were coated with a self-assembled monolayer (SAM, FOTS (1H, 1H, 2H, 2H – Perfluorooctyltrichlorosilane)) (AVC-150M, SORONA, Korea) as an antiadhesion layer for the easy molding of PDMS micropillar arrays of high AR. After the PDMS was cured at 85 °C on top of a hot plate for 4 h, the final thickness of the cured PDMS layer was 0.3 ± 0.02 mm.

Synthesis of ZnO NWs: To synthesize the vertically aligned ZnO NWs, ZnO nanocrystals (NCs) were used as nucleation sites. Using a syringe pump, sodium hydroxide (NaOH) (≥98%, Sigma-Aldrich) solution (0.03 M) in methanol was slowly added to 0.01 M of zinc acetate dihydrate (99.9%, Sigma-Aldrich) solution in methanol. Then, the mixture was vigorously stirred at 1500 rpm and 60 °C in an oil bath for 2 h. The obtained solution of ZnO NCs exhibited a semi-transparent color. Then, the ZnO NC solution was concentrated fivefold by evaporating the solvent. The concentrated ZnO NC solution was used for the dip-coating of uniform ZnO NCs onto the surface of micropillar-patterned PDMS substrates, which were treated with oxygen plasma and annealed at 100–150 °C on top of a hot plate for 20 min. It is noteworthy that these annealing and oxygen plasma treatments did not significantly affect to the flexibility of PDMS substrates. To prepare the growing solution for ZnO NWs, equimolar amounts (25×10^{-3} M) of $Zn(NO_3)_2 \cdot xH_2O$ (99.9%, Sigma-Aldrich) and HMTA (≥99.0%, Sigma-Aldrich) were mixed in DI water and dispersed by sonication. After preheating the growing solution for 5–10 min at 90 °C in a convection oven, the ZnO NCs-coated PDMS substrates were floated onto the surface of the growing solution.

Fabrication of Interlocked ZnO NW Arrays: To increase the electrical conductivity of ZnO NW arrays for the piezoresistive mode between the interlocked films, the ZnO NW arrays were coated with Pt (20-nm thick) by a metal-sputter coater (K575X sputter coater, Quorum Emitech., UK). For the piezoelectric mode of e-skins, only one layer of interlocked films was coated with a thick Ni layer (≈300 nm) (SRN-120M, SORONA, Korea). Then, the edge of the metal-coated ZnO NW arrays (1 cm × 1.5 cm) was attached to the copper (Cu) electrodes using silver paste.

Characterizations: The morphologies of the ZnO NWs and PDMS micropillar arrays were verified by field-emission scanning electron microscopy (FE-SEM) (S-4800, Hitachi, Japan). The crystal structure of ZnO NWs was characterized by using a high-resolution X-ray diffractometer (HR-XRD) (D8 Advance, Bruker, US). The variations in the electrical resistance of interlocking films were measured by using a two-probe method (4200-SCS, Keithley, US) with Cu electrodes attached to each layer of interlocked film. The applied voltage was 10 V. To evaluate the response time of ZnO NWs, an oscilloscope (DPO 2022B, Tektronix, US) was used at 1 μA of current using a two-probe method. The output current and voltage signals generated by the piezoelectric potential were characterized with a sourcemeter (2450-SCPI, Keithley, US). A pushing tester (JIPT-100, JUNIL TECH, Korea) was used to apply static and dynamic pressures onto the interlocked films. To investigate the levels of vibration and sound stimuli, a small coin-like vibration motor (DVM1034, Motorbank Co., Korea) was attached on the samples, and the vibrometer (ACO 3116, Guangzhou Orimay Electronic Co., Japan) was used to read the intensity of applied vibration. The measurement of acoustic vibration depending on the SPL was performed by reading the real-time change in SPL by using a commercial acoustimeter (TM-102, TENMARS, Taiwan).

Supporting Information

Supporting Information is available from the Wiley Online Library or from the author.

Acknowledgements

This work was supported by the Center for Advanced Soft Electronics under the Global Frontier Research Program (Grant No. 2012M3A6A5055728) and by the National Research Foundation of Korea (Grant No. NRF-2012K1A3A1A20031618) of the Ministry of Science, ICT & Future Planning, Korea.

Received: February 3, 2015
Revised: March 17, 2015
Published online: April 7, 2015

[1] S. Bauer, S. Bauer-Gogonea, I. Graz, M. Kaltenbrunner, C. Keplinger, R. Schwoediauer, *Adv. Mater.* **2014**, *26*, 149.
[2] M. L. Hammock, A. Chortos, B. C. K. Tee, J. B. H. Tok, Z. Bao, *Adv. Mater.* **2013**, *25*, 5997.

[3] J. Park, Y. Lee, J. Hong, M. Ha, Y. D. Jung, H. Lim, S. Y. Kim, H. Ko, *ACS Nano* **2014**, *8*, 4689.
[4] C. Pang, G. Y. Lee, T. I. Kim, S. M. Kim, H. N. Kim, S. H. Ahn, K. Y. Suh, *Nat. Mater.* **2012**, *11*, 795.
[5] X. Wang, Y. Gu, Z. Xiong, Z. Cui, T. Zhang, *Adv. Mater.* **2014**, *26*, 1336.
[6] Y. Wang, L. Wang, T. Yang, X. Li, X. Zang, M. Zhu, K. Wang, D. Wu, H. Zhu, *Adv. Funct. Mater.* **2014**, *24*, 4666.
[7] W. Honda, S. Harada, T. Arie, S. Akita, K. Takei, *Adv. Funct. Mater.* **2014**, *24*, 3299.
[8] S. Gong, W. Schwalb, Y. Wang, Y. Chen, Y. Tang, J. Si, B. Shirinzadeh, W. Cheng, *Nat. Commun.* **2014**, *5*, 3132.
[9] D. H. Kim, N. S. Lu, R. Ma, Y. S. Kim, R. H. Kim, S. D. Wang, J. Wu, S. M. Won, H. Tao, A. Islam, K. J. Yu, T. I. Kim, R. Chowdhury, M. Ying, L. Z. Xu, M. Li, H. J. Chung, H. Keum, M. McCormick, P. Liu, Y. W. Zhang, F. G. Omenetto, Y. G. Huang, T. Coleman, J. A. Rogers, *Science* **2011**, *333*, 838.
[10] R. Li, B. Nie, P. Digiglio, T. Pan, *Adv. Funct. Mater.* **2014**, *24*, 6195.
[11] D. P. Cotton, P. H. Chappell, A. Cranny, N. M. White, S. P. Beeby, *IEEE Sens. J.* **2007**, *7*, 752.
[12] H. Stoyanov, M. Kollosche, S. Risse, R. Waché, G. Kofod, *Adv. Mater.* **2013**, *25*, 578.
[13] G. T. Hwang, H. Park, J. H. Lee, S. Oh, K. I. Park, M. Byun, H. Park, G. Ahn, C. K. Jeong, K. No, H. Kwon, S. G. Lee, B. Joung, K. J. Lee, *Adv. Mater.* **2014**, *26*, 4880.
[14] J. Kim, M. Lee, H. J. Shim, R. Ghaffari, H. R. Cho, D. Son, Y. H. Jung, M. Soh, C. Choi, S. Jung, K. Chu, D. Jeon, S. T. Lee, J. H. Kim, S. H. Choi, T. Hyeon, D. H. Kim, *Nat. Commun.* **2014**, *5*, 11.
[15] D. Son, J. Lee, S. Qiao, R. Ghaffari, J. Kim, J. E. Lee, C. Song, S. J. Kim, D. J. Lee, S. W. Jun, S. Yang, M. Park, J. Shin, K. Do, M. Lee, K. Kang, C. S. Hwang, N. S. Lu, T. Hyeon, D. H. Kim, *Nat. Nanotechnol.* **2014**, *9*, 397.
[16] J. Dargahi, S. Najarian, *Int. J. Med. Robot.* **2004**, *1*, 23.
[17] A. B. Vallbo, R. S. Johansson, *Active Touch, the Mechanism of Recognition of Objects by Manipulation*, Pergamon Press Ltd., Oxford, England **1978**.
[18] D. G. Caldwell, N. Tsagarakis, A. Wardle, presented at *IEEE Int. Conf. Robot.*, Albuquerque, New Mexico **1997**.
[19] S. Littlejohn, A. Nogaret, G. M. Prentice, G. D. Pantos, *Adv. Funct. Mater.* **2013**, *23*, 5398.
[20] L. Viry, A. Levi, M. Totaro, A. Mondini, V. Mattoli, B. Mazzolai, L. Beccai, *Adv. Mater.* **2014**, *26*, 2659.
[21] B. C. K. Tee, A. Chortos, R. R. Dunn, G. Schwartz, E. Eason, Z. Bao, *Adv. Funct. Mater.* **2014**, *24*, 5427.
[22] H. Muhammad, C. Recchiuto, C. Oddo, L. Beccai, C. Anthony, M. Adams, M. Carrozza, M. Ward, *Microelectron. Eng.* **2011**, *88*, 1811.
[23] J. A. Dobrzynska, M. A. Gijs, *Sens. Actuators, A* **2012**, *173*, 127.
[24] J. Yang, J. Chen, Y. Liu, W. Yang, Y. Su, Z. L. Wang, *ACS Nano* **2014**, *8*, 2649.
[25] B. Chu, X. Zhou, K. Ren, B. Neese, M. Lin, Q. Wang, F. Bauer, Q. Zhang, *Science* **2006**, *313*, 334.
[26] K. Jung, J. Lee, M. Cho, J. C. Koo, Y. Lee, H. R. Choi, *Smart Mater. Struct.* **2007**, *16*, 288.
[27] W. Mai, Z. Liang, L. Zhang, X. Yu, P. Liu, H. Zhu, X. Cai, S. Tan, *Chem. Phys. Lett.* **2012**, *538*, 99.
[28] C. Metzger, E. Fleisch, J. Meyer, M. Dansachmueller, I. Graz, M. Kaltenbrunner, C. Keplinger, R. Schwoediauer, S. Bauer, *Appl. Phys. Lett.* **2008**, *92*, 013506.
[29] H.-K. Lee, S.-I. Chang, E. Yoon, *J. Microelectromech. Syst.* **2006**, *15*, 1681.
[30] M. Shimojo, A. Namiki, M. Ishikawa, R. Makino, K. Mabuchi, *IEEE Sens. J.* **2004**, *4*, 589.
[31] J. Zhang, S. Y. Zhang, S. Y. Feng, Z. G. Jiang, *Polym. Int.* **2005**, *54*, 1175.
[32] M.-J. Jiang, Z.-M. Dang, H.-P. Xu, *Appl. Phys. Lett.* **2006**, *89*, 182902.
[33] K. Autumn, Y. A. Liang, S. T. Hsieh, W. Zesch, W. P. Chan, T. W. Kenny, R. Fearing, R. J. Full, *Nature* **2000**, *405*, 681.
[34] S. N. Gorb, R. G. Beutel, E. V. Gorb, Y. K. Jiao, V. Kastner, S. Niederegger, V. L. Popov, M. Scherge, U. Schwarz, W. Votsch, *Integr. Comp. Biol.* **2002**, *42*, 1127.
[35] M. Spinner, G. Westhoff, S. N. Gorb, *Sci. Rep.* **2014**, *4*, 5481.
[36] Y. Hosoyamada, T. Sakai, *Anat. Embryol.* **2005**, *210*, 1.
[37] M. R. Maschmann, G. J. Ehlert, B. T. Dickinson, D. M. Phillips, C. W. Ray, G. W. Reich, J. W. Baur, *Adv. Mater.* **2014**, *26*, 3230.
[38] O. Dangles, D. Pierre, C. Magal, F. Vannier, J. Casas, *J. Exp. Biol.* **2006**, *209*, 4363.
[39] J. M. CAMHI, *J. Exp. Biol.* **1970**, *52*, 519.
[40] S. Sterbing-D'Angelo, M. Chadha, C. Chiu, B. Falk, W. Xian, J. Barcelo, J. M. Zook, C. F. Moss, *Proc. Natl. Acad. Sci. U.S.A.* **2011**, *108*, 11291.
[41] J. Park, Y. Lee, J. Hong, Y. Lee, M. Ha, Y. Jung, H. Lim, S. Y. Kim, H. Ko, *ACS Nano* **2014**, *8*, 12020.
[42] Y. Y. Wu, H. Q. Yan, M. Huang, B. Messer, J. H. Song, P. D. Yang, *Chem. Eur. J.* **2002**, *8*, 1261.
[43] L. E. Greene, M. Law, J. Goldberger, F. Kim, J. C. Johnson, Y. F. Zhang, R. J. Saykally, P. D. Yang, *Angew. Chem. Int. Ed.* **2003**, *42*, 3031.
[44] Z. Y. Fan, J. G. Lu, *Appl. Phys. Lett.* **2005**, *86*, 032111.
[45] U. Ozgur, Y. I. Alivov, C. Liu, A. Teke, M. A. Reshchikov, S. Dogan, V. Avrutin, S. J. Cho, H. Morkoc, *J. Appl. Phys.* **2005**, *98*, 041301.
[46] J. Archard, *Proc. R. Soc. London A* **1957**, *243*, 190.
[47] S. C. B. Mannsfeld, B. C. K. Tee, R. M. Stoltenberg, C. V. H. H. Chen, S. Barman, B. V. O. Muir, A. N. Sokolov, C. Reese, Z. N. Bao, *Nat. Mater.* **2010**, *9*, 859.
[48] A. Mikrajuddin, F. G. Shi, H. K. Kim, K. Okuyama, *Mater. Sci. Semicond. Process.* **1999**, *2*, 321.
[49] R. El Abdi, N. Benjemaa, *Int. J. Syst. Appl., Eng. Dev.* **2008**, *2*, 75.
[50] K. H. Nam, I. H. Park, S. H. Ko, *Nature* **2012**, *485*, 221.
[51] S. Kumar, W. A. Curtin, *Mater. Today* **2007**, *10*, 34.
[52] P. J. Pauzauskie, P. Yang, *Mater. Today* **2006**, *9*, 36.
[53] P. C. A. Kam, A. C. Kam, J. F. Thompson, *Anaesthesia* **1994**, *49*, 982.
[54] J. Yang, J. Chen, Y. Liu, W. Q. Yang, Y. J. Su, Z. L. Wang, *ACS Nano* **2014**, *8*, 2649.
[55] S. N. Cha, J. S. Seo, S. M. Kim, H. J. Kim, Y. J. Park, S. W. Kim, J. M. Kim, *Adv. Mater.* **2010**, *22*, 4726.
[56] W. Z. Wu, X. N. Wen, Z. L. Wang, *Science* **2013**, *340*, 952.
[57] C. F. Pan, L. Dong, G. Zhu, S. M. Niu, R. M. Yu, Q. Yang, Y. Liu, Z. L. Wang, *Nat. Photonics* **2013**, *7*, 752.
[58] R. D. Kingsmith, D. Vanderbilt, *Phys. Rev. B* **1993**, *47*, 1651.
[59] Z. L. Wang, J. H. Song, *Science* **2006**, *312*, 242.
[60] Y. Qin, X. D. Wang, Z. L. Wang, *Nature* **2008**, *451*, 809.
[61] S. Xu, Y. Qin, C. Xu, Y. G. Wei, R. S. Yang, Z. L. Wang, *Nat. Nanotechnol.* **2010**, *5*, 366.
[62] S. Wang, L. Lin, Z. L. Wang, *Nano Energy* **2015**, *11*, 436.
[63] J. K. Otto, T. D. Brown, J. J. Callaghan, *Exp. Mech.* **1999**, *39*, 317.
[64] J. Sirohi, I. Chopra, *J. Intell. Mater. Syst. Struct.* **2000**, *11*, 246.
[65] S. Y. Xu, Y. W. Yeh, G. Poirier, M. C. McAlpine, R. A. Register, N. Yao, *Nano Lett.* **2013**, *13*, 2393.
[66] R. Zhu, D. Wang, S. Xiang, Z. Zhou, X. Ye, *Nanotechnology* **2008**, *19*, 285712.
[67] N. Jalali, P. Woolliams, M. Stewart, P. M. Weaver, M. G. Cain, S. Dunn, J. Briscoe, *J. Mater. Chem. A* **2014**, *2*, 10945.
[68] Y. Mao, P. Zhao, G. McConohy, H. Yang, Y. Tong, X. Wang, *Adv. Energy Mater.* **2014**, *4*, 1301624.
[69] X.-S. Zhang, M.-D. Han, R.-X. Wang, F.-Y. Zhu, Z.-H. Li, W. Wang, H.-X. Zhang, *Nano Lett.* **2013**, *13*, 1168.
[70] S. Yun, S. Park, B. Park, Y. Kim, S. K. Park, S. Nam, K.-U. Kyung, *Adv. Mater.* **2014**, *26*, 4474.